Cambridge Centre for Computational Chemical Engineering

University of Cambridge

Department of Chemical Engineering

Modes of Neck Growth in Nanoparticle Aggregates

Neal M Morgan, Robert I A Patterson, Abhijeet Raj and Markus Kraft [1]

released: 23 February 2007

[1] Department of Chemical Engineering
University of Cambridge
Pembroke Street, Cambridge
CB2 3RA, UK
E-mail: mk306@cam.ac.uk

c4e

Abstract

In this work we investigate the effect of non-uniform surface growth on flame generated nanoparticle aggregates. Two models are considered for the change in shape of a two unit aggregate gaining mass through surface reactions in order to answer a question from [Balthasar & Frenklach, Proc. Combust. Inst. 30(2005), 1467]. The first model, taken from the literature, represents the primary particles, which comprise an aggregate, as uniformly expanding, overlapping spheres. A second, new model is introduced, in which all growth is concentrated on the formation of a frustum between the two primary particles and used to test the importance of the uniform growth assumption. The effects of both models are investigated for soot formation in laminar premixed flames and are shown to predict significant differences in particle shape for a number of systems. The comparison was performed by calculating the percentage increase in mass needed to return a newly formed two unit aggregate to different levels of sphericity for both models, and collecting values for this percentage from simulations of premixed laminar flames.

1 Introduction

This short article provides an answer to a question[1] about the effect of preferential locations for surface reactions on flame-generated, aggregate nanoparticles asked when the paper by Balthasar and Frenklach [3] was presented at the 30th International Symposium on Combustion. The work in [3] concerned very detailed simulations of soot particle populations in laminar premixed flames, which built on the methods developed in [12, 13]. In that work very detailed models of the aggregate structures of soot particles were represented by unions of intersecting spheres.

The model used in [3] is that soot particles form when small solid particles are incepted from the gas phase. Particles can then grow (or shrink and burn up) and coagulate. Immediately after coagulation, particles are assumed to be in approximately point contact, thus there is a narrow neck and a small zone where the surfaces of the two particles are very close together. The questioner asked what would happen if "the 'saddle-shaped' region where two particles touch was either: a.) a preferred site for growth (as in the case of capillary condensation) or, alternately b.) relatively 'inaccessible' ". The original work [3] had assumed that surface reactions were evenly distributed over the free surface area of all primary particles; the relevant part of the model is summarised in section 2.1.

Preferential surface growth (if particles are to form then growth reactions must initially predominate) around the point of contact between two newly joined particles would lead to a more rapid build of the join between them. It might also affect the amount of surface growth required to build the two newly coagulated particles into one larger, approximately spherical particle. That such rounding out takes place is well established since TEMs of soot particles, such as those in [15] and [25], show the soot to be composed of a modest number of so called primary particles with diameters of the order of 20 nm. Since soot particles contain graphitic material [26] and substantial numbers of large polyaromatic hydrocarbon molecules [1, 3], which are unlikely to exhibit liquid like flow or diffusion, the formation of frustums between primary particles would have to be explained in terms of the neck region being a preferred reaction site for surface growth processes. For inorganic nanoparticles, surface diffusion and flow could play a role in building frustums, in addition to any effects of preferred reaction sites. Recently there has been some evidence that aliphatic species can also be observed in soot particles. These aliphatic molecules have higher mobility than the large PAH units and might be subject to surface diffusion, which in turn would lead to 'liquid properties' for the soot particle [28]. However from the data available it is unclear how important this effect is. Due to the focus on soot particles in the present work, only preferred reaction sites will be considered. For information on sintering in inorganic nanoparticles see [21], the detailed modelling studies in [10] and the references of those papers.

In this article the expanding and overlapping sphere model used for surface growth in the initial work [3] will be briefly reviewed. Then a new model, the 'Conical Frustum' model, which concentrates the growth in the necks between newly coagulated particles will be presented. Finally, the differences between the two models will be assessed by considering the amount of mass required to build two spheres in point contact up into an

---

[1]The symposium proceedings [3] include a record of this question; it appears after the references, as the first item on page 1475.

approximately spherical shape.

2 Surface Growth Models

Figure 1 shows a dimer (two primary element) particle at the moment after coagulation. Let the left-hand and right-hand spheres have initial radii, $r_{1,0}$ and $r_{2,0}$ respectively. The
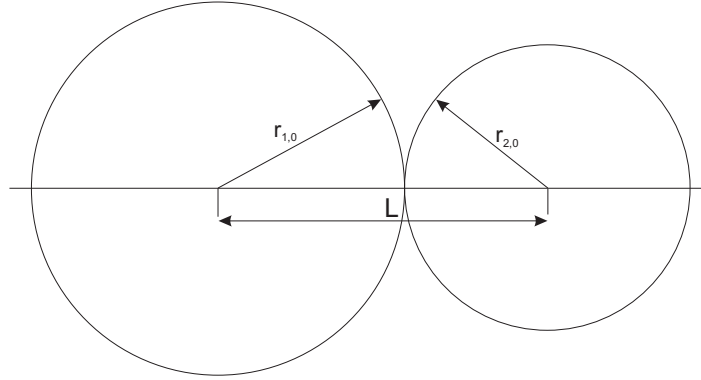
Figure 1: *Diagram of the dimer particle*

distance between the centres of the two spheres is $L = r_{1,0} + r_{2,0}$.

The dimer will have an initial volume of

$$v_0 = \frac{4\pi}{3} \left(r_{1,0}^3 + r_{2,0}^3 \right), \tag{1}$$

and a surface area of

$$a_0 = 4\pi \left(r_{1,0}^2 + r_{2,0}^2 \right). \tag{2}$$

The sphericity (the inverse of the ratio of the actual surface area to that of a sphere with the same volume[2]) is then

$$\psi = \frac{\pi^{\frac{1}{3}} \left(6v_0 \right)^{\frac{2}{3}}}{a_0}. \tag{3}$$

Two models will now be considered for the way new material can be added to the surface of the dimer of figure 1. First the original, Overlapping Spheres model will be reviewed.

2.1 Overlapping Spheres (OS)

Figure 2 shows the spheres after a certain amount of surface growth, which is simply modelled as an increase in radii from $r_{1,0}$ and $r_{2,0}$, to r_1 and r_2. No new material is required to expand the section of each particle that is already enclosed by the other, but these enclosed regions do not have a free surface so they cannot participate in surface

---

[2]A sphere has sphericity 1, a long thin shape will have sphericity only a little greater than 0.

3

growth. The notional internal boundaries are drawn in figure 2 to make the size of the overlap between the two spheres clear.
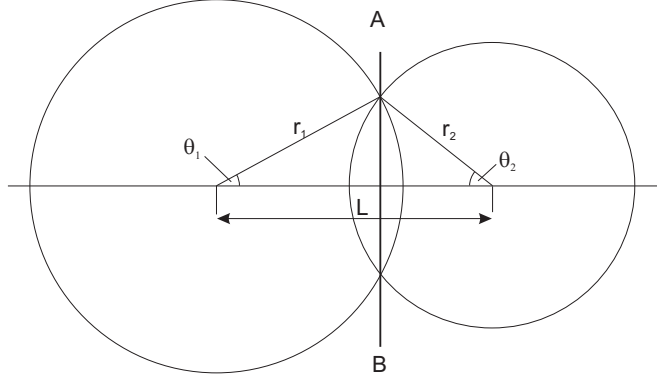
Figure 2: *Diagram of the dimer particle with partially-overlapping radii.*

The angles, θ_1 and θ_2 from figure 2 can be determined by applying the cosine rule to the triangle of lengths r_1, r_2 and L. One obtains

$$\cos(\theta_1) = \frac{r_1^2 + L^2 - r_2^2}{2r_1 L} \quad \text{and} \quad \cos(\theta_2) = \frac{r_2^2 + L^2 - r_1^2}{2r_2 L}. \tag{4}$$

The volumes to the left ($n = 1$) and right ($n = 2$) of the line AB may be obtained from a volume integral or by combining standard formulæ to get

$$v_{\text{SphSect},n} = \pi r_n^3 \left[\frac{2}{3} + \cos(\theta_n) - \frac{\cos^3(\theta_n)}{3} \right] , \quad n = 1, 2. \tag{5}$$

In a similar way, the surface areas are:

$$a_{\text{SphSect},n} = 2\pi r_n^2 \left(\cos(\theta_n) + 1 \right) , \quad n = 1, 2. \tag{6}$$

2.2 Conical Frustum Growth (CF)

Figure 3 is a schematic representation of the dimer undergoing initial conical frustum growth. The angle $\phi_1 \in [0, \Phi]$ (given in radians) is a variable used to describe the extent of the frustum growth. Φ is the maximum possible angle for a conical frustum. By simple geometry

$$\cos(\Phi) = \frac{r_1 - r_2}{L}. \tag{7}$$

To prevent unrealistic frustum shapes ϕ_1 and ϕ_2 are coupled by requiring them both to take up the same fraction of their maximum possible value, that is,

$$\phi_2 = \phi_1 \frac{\pi - \Phi}{\Phi}. \tag{8}$$

4
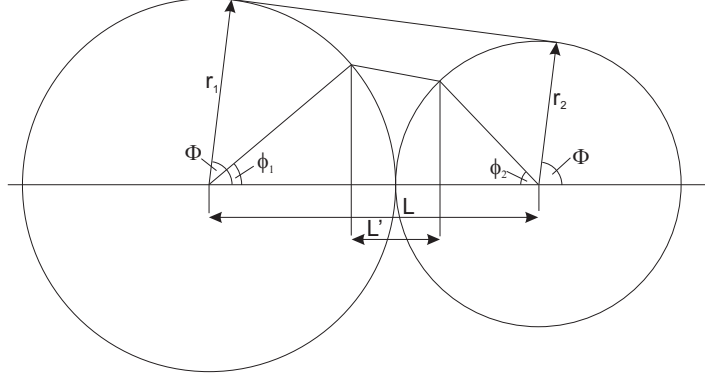
Figure 3: *Diagram of the dimer particle with partial conical frustum.*

In particular, this linear expression ensures that ϕ_1 and ϕ_2 are both 0 together and take their maximum values together.

The total volume of a particle with a conical frustum defined by the angle ϕ_1 can be calculated by dividing the shape into three regions divided by two vertical lines (planes) running through the points where the ends of the frustum touch the surfaces of the spheres. The volume of the two outer regions is then found from (5) by replacing θ_n with ϕ_n, The (horizontal) length of the frustum, L', is

$$L' = L - r_1 \cos(\phi_1) - r_2 \cos(\phi_2). \tag{9}$$

The equation of a straight line, $y = mx + c$, connecting the ends of the frustum is easy to calculate and a volume of revolution integration can then be performed showing that the volume of the conical frustum is

$$v_{\text{frustum}} = \pi \int_0^{L'} (mx + c)^2 \, \mathrm{d}x = \pi \left(\frac{m^2 L'^3}{3} + mcL'^2 + c^2 L' \right). \tag{10}$$

and so the total volume of the particle is given by

$$v = v_{\text{SphSect,1}} + v_{\text{SphSect,2}} + v_{\text{frustum}}. \tag{11}$$

The surface area of the conical frustum can be determined by a surface integral:

$$a_{\text{frustum}} = \pi \left[r_1 \sin(\phi_1) + r_2 \sin(\phi_2) \right] \times \sqrt{(r_1 \sin(\phi_1) - r_2 \sin(\phi_2))^2 + L'^2}. \tag{12}$$

The surface areas of the spherical sectors are found from (6), again replacing θ_n with ϕ_n. The total area of the particle is found as

$$a = a_{\text{SphSect,1}} + a_{\text{SphSect,2}} + a_{\text{frustum}}. \tag{13}$$

When the frustum has grown such that $\phi_1 = \Phi$, we enter a secondary growth regime for the particle. Figure 4 shows the growth of the particle in this state. When this happens the volumes and area of the shape are calculated from (5), (6), (10), (11), (12) and (13) with the angles ϕ_1 and ϕ_2 replaced by Φ and $\pi - \Phi$ respectively.

5
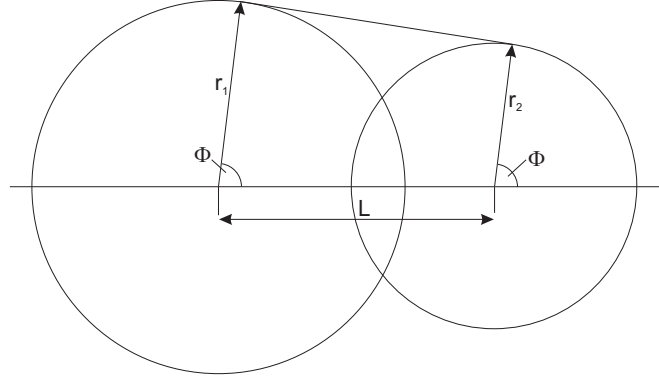
Figure 4: *Diagram of the dimer particle with full conical frustum and further growth.*

3 Results and Discussion

The two models outlined above were analysed in terms of change in sphericity (see (3)) and the mass change of particles expressed as a fraction of their initial mass. For a particle of initial mass m gaining an amount of mass $\triangle m$ let the fractional change in mass be denoted by

$$\xi = \frac{\triangle m}{m}. \tag{14}$$

3.1 Idealised Analysis

Two different initial dimer configurations were considered. In the first case, the radii of both sub-particles were equal ($r_{1,0} = r_{2,0} = 1$). In the second case, the radii were different, ($r_{1,0} = 2, r_{2,0} = 1$).

Figure 5 shows how ξ and the sphericity, ψ are related for the first case and how the two models from section 2 differ from each other. The initial condition is $\psi = 0.794$. It is clear from the graphs that the CF model requires much less mass to raise the sphericity of the dimer to any value below 0.98 than the OS model. For example, if $\xi = 1$, the OS model produces a sphericity of 0.87, whereas the CF model produces 0.94. As might be expected there is a discontinuity in the gradient of the CF curve at the point where frustum growth is complete. After this point the CF model behaves in a similar manner to the OS model and the curves rapidly converge.

Figure 6 shows the response of sphericity to ξ for the second case, where one particle had twice the initial radius of the other. In this case the initial condition is $\psi = 0.865$. As before, it is clear the CF model requires less mass to convert the dimer to near-sphericity than the OS model.

Once the radii of the two particles forming a dimer differ by a factor of more than 3 the sphericity of the dimer will exceed 0.9. For such particles the amount of mass required to complete the frustum is relatively small and the regime in which the CF and OS models converge would be reached quickly. Therefore the above analysis was not extended to
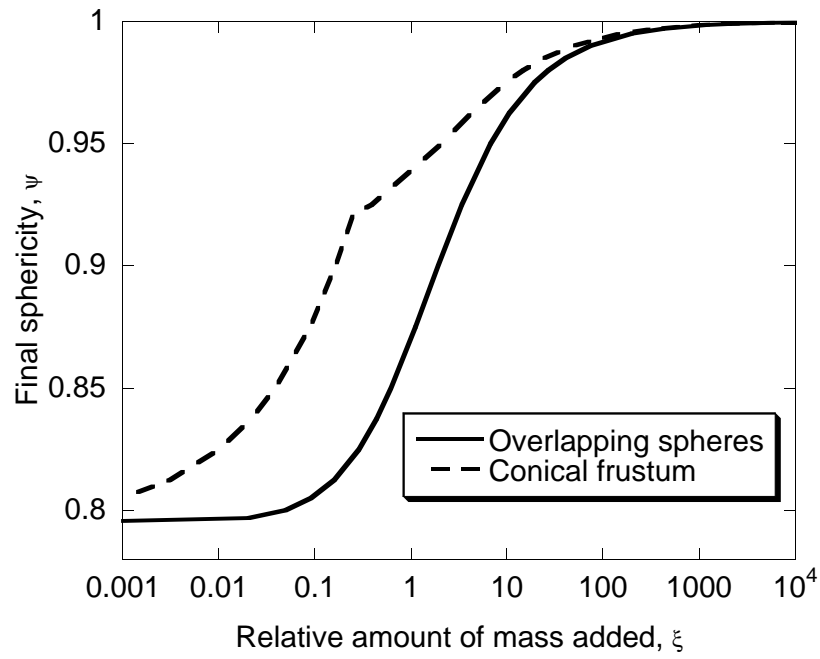
Figure 5: *The variation of ξ with ψ for two particles of equal size ($r_{1,0} = r_{2,0} = 1$).*
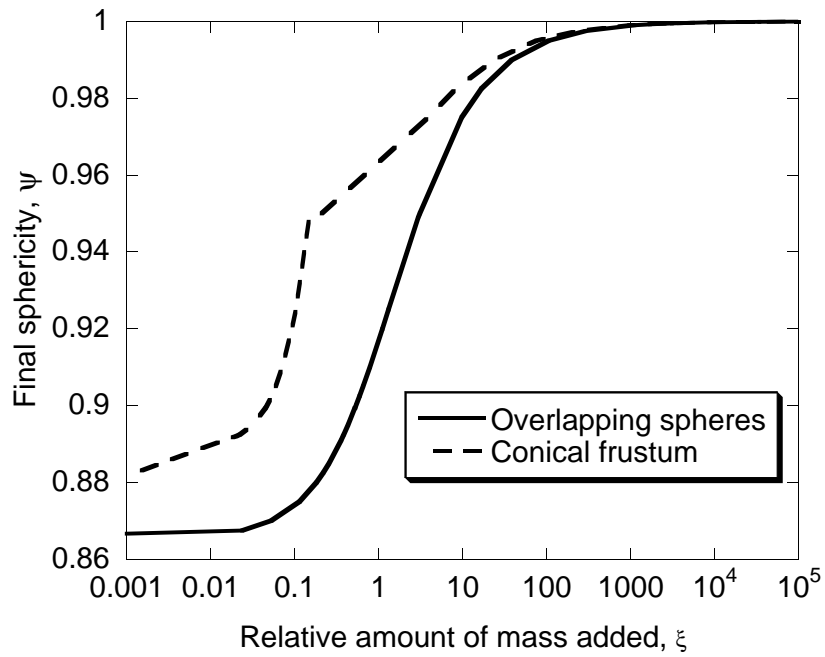
Figure 6: *The variation of ξ with ψ for two particles of $r_{1,0} = 2$, $r_{2,0} = 1$.*

ratios of more than 2:1.

The above results suggest that preferential growth around the points of contact between sub-units within an aggregate would lead to significantly different aggregate structures to those that would form if growth were evenly distributed over all the free surface of an aggregate. The differences in the size of the connections between primary particles will be greatest when large numbers of similarly sized particles are incepted in a short space of time and then quickly move to a location where there is little surface growth. The differences will be much smaller if inception is spread over a longer period of time so that, in general, coagulation will join a small particle to a large one and if surface growth leads to a high mass addition rate over an extended period of time. In summary, preferential growth at points of contact between aggregate sub-units would lead to rounder particles in situations where surface growth occurs at a low rate or where nucleation is intense and brief, for example in the flame JW10.673 considered below, but make little difference to flames with abundant surface growth such as HWA3, also considered below.

Figures 5&6 also show that the two models will predict similar surface areas for particles, because the ratio of ψ for two particles of the same mass is the inverse of the ratio of their surface areas. Since growth reactions on particle surfaces are the main route for soot mass increase [16] and figures 5&6 indicate a maximum difference in surface area of under 15% the difference in growth rates between the OS and CF models is also unlikely to exceed 15%. The two models will therefore predict similar soot volume fractions.

Examination of figure 6 suggests that the key region of difference between the frustum and overlapping spheres models for surface growth is $0.03 < \xi < 1$. Accordingly estimates of the values of ξ applicable to soot particles in premixed laminar flames are presented.

3.2   Estimates of ξ for Physical Systems

Values of ξ were tracked in simulations using the soot model and accelerated direct simulation Monte Carlo algorithm from [2, 16, 17, 19]. Values averaged across the particle populations are plotted for a range of premixed flames in figure 7. A summary of the flame conditions simulated is given in table 1. Simulations of DLR6 were stopped just above the stabilizing grid used in the experiments [22].

Table 1: *Summary of simulated flames.*

name	P / bar	equiv. ratio	simulated height / cm	reference
JW10.673	10	2.02	3.4	[9]
DLR6	5	2.4	3.6	[22]
HWA3	1	1.92	1.3	[27]
HWA1	1	1.92	1.2	[27]
JW1.69	1	2.07	4.1	[9]

When considering the data in figure 7 one should note that what is shown is the average across all particles in the flames. Particles that have just been formed by inception or
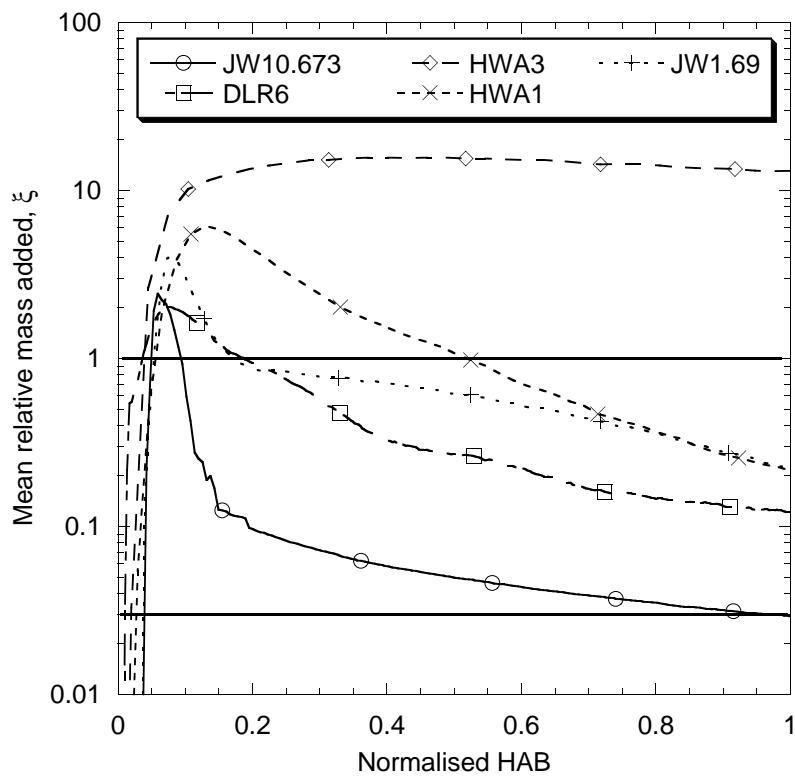
Figure 7: *Population average ξ for laminar premixed ethylene flames as fraction of distance from burner to assumed top of flame.*

9

coagulation will have small values of ξ. Large particles will tend to have smaller values of ξ than small particles because they will have a lower surface to volume ratio. This correlation can be clearly seen in figure 8, where a bimodal size distribution corresponds to a bimodal ξ distribution. Far from the burner surface the other flames considered also
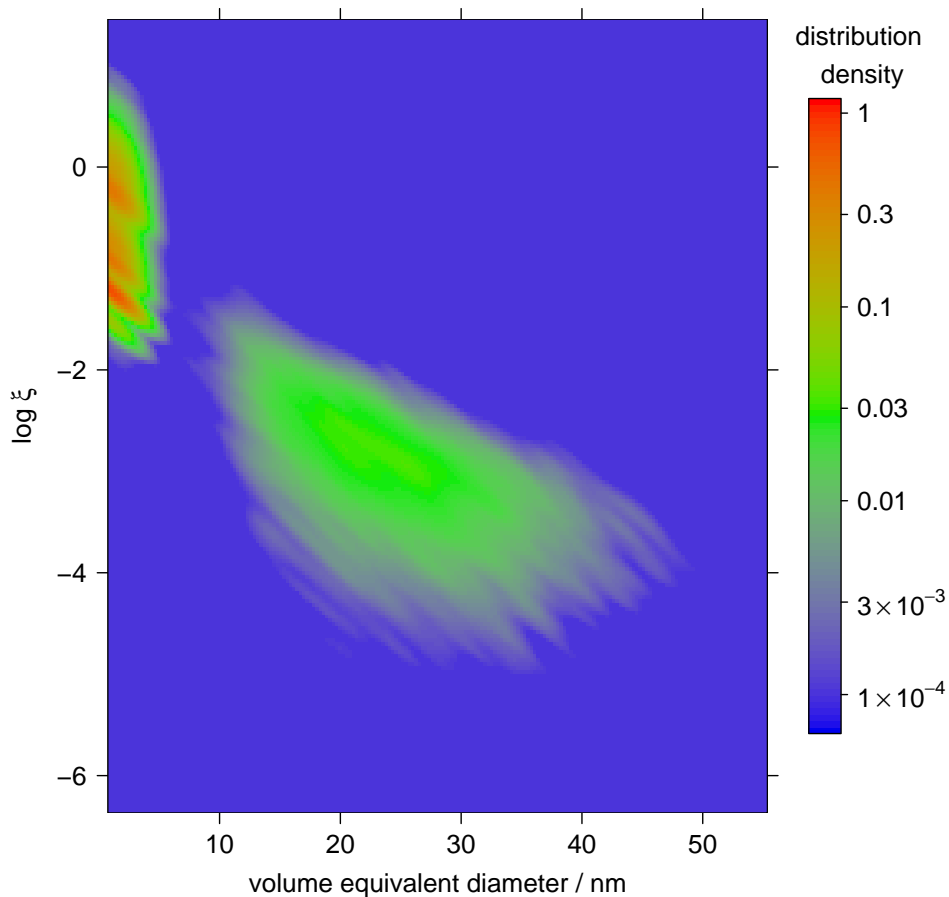
Figure 8: *ξ and diameter distribution at top of JW1.69.*

have a similar diagonal structure to that seen far from the burner surface of JW1.69 in figure 8; although the flames with unimodal size distributions at these distances naturally do not have the second peak seen at the very left of figure 8.

Another way to explore the size—ξ correlation is to consider mass weighted averages instead of the number weighted averages used in figure 7. For all the flames considered the mass weighted average of ξ was lower than the number weighted average, typically by a factor of around 10 at the end of the flame.

The simulated values of ξ show that a significant number of particles are likely to be in the critical $0.03 < \xi < 1$ region throughout many, but not all, premixed laminar flames with light hydrocarbon fuels. Therefore, for most flames, the overlapping spheres model would predict the onset of aggregation earlier than the frustum model. Soot particles in diffusion

flames also move from rich to lean conditions [8] and so pass through the critical ξ region and, provided the transition is not too rapid, the choice of model will be significant for this type of flame too.

In principle it should be possible to choose between the two models by seeing which best predicts particle structures sampled from different flame positions. TEM techniques for this are well developed [20] and AFM has also been used [4]. However, such comparisons would be heavily influenced by the surface growth rates predicted by the soot and flame chemistry model used and the chemistry of sooting systems is an active area of research [6, 7, 11, 24]. A general conclusion on which of the two models considered in this paper is to be preferred for flame simulation will therefore not be possible until quite accurate models are available for a range of flames. These models will need to include the surface growth rates involving a range of chemical species and the structure of soot particles. Theoretical [5, 23, 24] and experimental [14, 26] efforts are in progress to reach this goal.

3.3 Cancellation of Growth and Oxidation

Implicit in (14), and in the work using the overlapping spheres model [3, 13], is the assumption that surface growth and oxidation may be cancelled against each other before calculating the change in particle shape. This is quite an important assumption because the processes are quite finely balanced. For the flame HWA3 the mass addition and removal differ by no more than one part in 10^4. Other work by the current authors, with a less detailed model of particle shape [18], indicates that separate distributions of surface growth and oxidation can make a 20% difference to the total particle surface area. This difference arises in the initial stages of a flame and persists to the end of the flame along with an approximately proportional increase in soot mass.

4 Conclusion

The answer to the question from the 30th Symposium is that, if the model, to which the question referred, is changed only by concentrating all surface reactions at the necks between the primary particles making up aggregates, then the flame position and particle size at which aggregations is predicted to start will be affected. However, the soot volume fraction would not be significantly changed.

5 Acknowledgements

References

[1] B Apicella, A Carpentieri, M Alfè, R Barbella, A Tregrossi, P Pucci, and A Ciajolo. Mass spectrometric analysis of large PAH in a fuel-rich ethylene flame. *Proc. Combust. Inst.*, 31(1):547–553, 2001.

[2] M Balthasar and M Kraft. A stochastic approach to solve the particle size distribution function of soot particles in laminar premixed flames. *Combust. Flame*, 133:289–298, 2003.

[3] Michael Balthasar and Michael Frenklach. Monte-Carlo simulation of soot particle coagulation and aggregation: the effect of a realistic size distribution. *Proc. Combust. Inst.*, (30):1467–1475, 2005.

[4] A C Barone, A D'Alessio, and A D'Anna. Morphological characterization of the early process of soot formation by atomic force microscopy. *Combust. Flame*, 132: 181–187, 2003.

[5] Michael Frenklach, Charles A Schuetz, and Jonathan Ping. Migration mechanism of aromatic-edge growth. *Proc. Combust. Inst.*, 30:1389–1396, 2005. doi:10.1016/j.proci.2004.07.048.

[6] Karlheinz Hoyermann, Fabian Mauß, and Thomas Zeuch. A detailed chemical reaction mechanism for the oxidation of hydrocarbons and its application to the analysis of benzene formation in fuel-rich premixed laminar acetylene and propene flames. *Phys. Chem. Chem. Phys.*, 6:3824–3835, 2004. doi:10.1039/b404632c.

[7] Sergei Izvekov and Angela Violi. A coarse-grained molecular dynamics study of carbon nanoparticle aggregation. *J. Chem. Theory Comput.*, 2:504–512, 2005. doi:10.1021/ct060030d.

[8] C R Kaplan and K Kailasanath. Flow-field effects on soot formation in normal and inverse methane-air diffusion flames. *Combust. Flame*, 124:275–294, 2001.

[9] A Kazakov, H Wang, and M Frenklach. Detailed modeling of soot formation in laminar premixed ethylene flames at a pressure of 10 bar. *Combust. Flame*, 100: 111–120, 1995.

[10] M Kostoglou, A G Konstandopoulos, and S K Friedlander. Bivariate population dynamics simulation of fractal aerosol aggregate coagulation and restructuring. *J. Aerosol Sci.*, 37:1102–1115, 2006. doi:10.1016/j.jaerosci.2005.11.009.

[11] J C Lee, H N Najm, S Lefantzi, J Ray, M Frenklach, M Valorani, and D A Goussis. A CSP and tabulation-based adaptive chemistry model. *Combust. Theor. Model.*, 2007.

[12] P A Mitchell. *Monte Carlo Simulation of Soot Aggregation with Simultaneous Surface Growth*. PhD thesis, University of California, Berkeley, 2001.

[13] Pablo Mitchell and Michael Frenklach. Particle aggregation with simultaneous surface growth. *Phys. Rev. E*, 67:061407, 2003.

[14] I Morjan, I Voicu, F Dumitrache, I Sandu, I Soare, R Alexandrescu, E Vasile, I Pasuk, R M D Brydson, H Daniels, and B Rand. Carbon nanopowders from the continuous-wave CO_2 laser-induced pyrolysis of ethylene. *Carbon*, 41:2913–2921, 2003. doi:10.1016/S0008-6223(03)00381-6.

[15] Berk Öktem, Michael P Tolocka, Bin Zhao, Hai Wang, and Murray V Johnston. Chemical species associated with the early stage of soot growth in a laminar premixed ethylene-oxygen-argon flame. *Combust. Flame*, 142:364–373, 2005.

[16] R I A Patterson, J Singh, M Balthasar, M Kraft, and J R Norris. The linear process deferment algorithm: A new technique for solving population balance equations. *SIAM J. Sci. Comput.*, 145(1):303–320, 2006.

[17] Robert Patterson, Jasdeep Singh, Michael Balthasar, Markus Kraft, and Wolfgang Wagner. Extending stochastic soot simulation to higher pressures. *Combust. Flame*, 145(3):638–642, 2006.

[18] Robert Patterson, Jasdeep Singh, Neal Morgan, and Markus Kraft. A simple model for the aggregate structure of soot particles. Technical Report 38, c4e Preprint-Series, Cambridge, 2006.

[19] J Singh, R Patterson, M Balthasar, M Kraft, and W Wagner. Modelling soot particle size distribution: Dynamics of pressure regimes. Technical Report 25, c4e Preprint-Series, Cambridge, 2004.

[20] Kuo Tian, Fengshan Liu, Min Yang, Kevin A Thomson, David R Snelling, and Gregory J Smallwood. Numerical simulation aided relative optical density analysis of TEM images for soot morphology determination. *Proc. Combust. Inst.*, 31(1): 861–868, 2007.

[21] Stavros Tsantilis and Sotiris E Pratsinis. Soft- and hard-agglomerate aerosols made at high temperatures. *Langmuir*, 20(14):5933–5939, 2004.

[22] M S Tsurikov, K P Geigle, V Krüger, Y Schneider-Kühnle, W Stricker, R Lückerath, R Hadef, and M Aigner. Laser-based investigation of soot formation in laminar premixed flames at atmospheric and elevated pressures. *Combust. Sci. Tech.*, 177: 1835–1862, 2005. doi:10.1080/00102200590970212.

[23] Angela Violi, Gregory A Voth, and Adel F Sarofim. The relative roles of acetylene and aromatic precursors during soot particle inception. *Proc. Combust. Inst.*, 30(1): 1343–1351, 2005. doi:10.1016/j.proci.2004.08.226.

[24] Russell Whitesides, Alexander C Kollias, Dominik Domin, William A Lester, jr, and Michael Frenklach. Graphene layer growth: Collision of migrating five-member rings. *Proc. Combust. Inst.*, 31(1):539–546, 2007.

[25] F Xu, K C Lin, and G M Faeth. Soot formation in laminar premixed methane/oxygen flames at atmospheric pressure. *Combust. Flame*, 115:195–209, 1998.

[26] Shihong Yan, Yi-Jin Jiang, Nathan D Marsh, Eric G Eddings, Adel F Sarofim, and Ronald J Pugmire. Study of the evolution of soot from various fuels. *Energy & Fuels*, 19:1804–1811, 2005.

[27] Bin Zhao, Zhiwei Yang, Zhigang Li, Murray V Johnston, and Hai Wang. Particle size distribution function of incipient soot in laminar premixed ethylene flames: effect of flame temperature. *Proc. Combust. Inst.*, 30:1441–1448, 2005.

[28] Bin Zhao, Kei Uchikawa, and Hai Wang. A comparative study of nanoparticles in premixed flames by scanning mobility particle sizer, small angle neutron scattering, and transmission electron microscopy. *Proc. Combust. Inst.*, 31(1):851–860, 2007.